Building and Environment 193 (2021) 107460

Contents lists available at ScienceDirect

Building and Environment

journal homepage: http://www.elsevier.com/locate/buildenv

Assessment of moisture risk of wooden beam embedded in internally insulated masonry walls with 2D and 3D models

Xiaohai Zhou [a,b,*], Jan Carmeliet [b], Dominique Derome [c]

[a] Laboratory of Multiscale Studies in Building Physics, Empa, Dübendorf, Switzerland
[b] Chair of Building Physics, ETH Zürich, Zürich, Switzerland
[c] Department of Civil and Building Engineering, Université de Sherbrooke, Sherbrooke, Canada

ARTICLE INFO

Keywords:
Interior thermal insulation
Clay brick masonry wall
Wooden beam-end
Hygrothermal model
2D and 3D modelling

ABSTRACT

Internal insulation of masonry walls may significantly increase the decay risk of embedded wooden beams due to lower temperature and consequently lower drying potential in retrofitted existing walls. Since high moisture contents will affect performance and service life of wood, the assessment of moisture-related damage risks in wooden beam-ends in internally insulated masonry walls is particularly relevant to heritage buildings. The proper selection of indoor and outdoor materials and the addition of an embedded heating source offer means of decreasing this risk. Numerical studies of hygrothermal performance of wooden beam-ends support risk assessment but traditionally this has been performed with 2D models. Therefore, in order to assess whether a 2D numerical model can represent accurately the 3D hygrothermal behavior of wooden beam-ends, the difference between 2D and 3D model results of the hygrothermal performance of wooden beam-ends embedded in internally insulated masonry wall is analysed for a northern continental climate. Given the small differences in relative humidity, temperature and mould index between the 2D and 3D models, it is suitable to replace 3D models with 2D ones for predicting the risk of moisture-related problems in the wood beam-end when studying the impact of different envelope components. However, for evaluating the effect of active heating on wooden beam-end performance, it is found that a 3D hygrothermal model should be used. In this case, a 2D model cannot accurately model heating locally at the beam-end resulting in an over prediction of temperature and thus in an underprediction of the moisture damage risk.

1. Introduction

Many historical buildings are built with solid brick walls and wooden beam constructions. These buildings are, for the most part, not energy efficient and represent a significant energy-saving potential. For historical buildings with a worth-preserving facade, the only possible energy retrofit measure possible given their heritage value is internal wall insulation. It is possible to reduce the heating energy consumption in the historical buildings by 30–40% by retrofitting the existing walls with internal insulation [1]. However, adding insulation to masonry walls from the indoor side may significantly increase moisture-related damage risks to the building materials and components that are exposed to lower temperature and consequently lower drying potential in the existing wall [2–10]. As the floors in old masonry buildings are often carried by wooden beams embedded in the brick masonry, moisture-related problems in wooden beam-ends in internally insulated masonry walls is of high practical importance [11] and should be correctly evaluated [12].

Moisture play an important role on the durability of building envelopes [13–15]. Wind-driven rain is the most important moisture source to building envelopes. High wind-driven rain loads onto load-bearing masonry walls can lead to high moisture contents and eventually to the decay of wooden beam-ends embedded in such walls. Sustained exposure to conditions resulting in high moisture content can lead to wood biodegradation and affect wood performance and service life. Mould growth on moist wooden surfaces will produce large numbers of spores, give off unpleasant odors and impair air quality, while wood rot results in decomposition and loss of mechanical properties [16]. Means of control can be passive by material selection or active, i.e. with local heating. Hence, field investigations and numerical studies indicate that the exterior render of masonry walls affects water uptake during wind driving rain events [3,6,17,18]. Exterior renders with high liquid water

* Corresponding author. Laboratory of Multiscale Studies in Building Physics, Empa, Dübendorf, Switzerland.
E-mail address: xiaohai.zhou@empa.ch (X. Zhou).

https://doi.org/10.1016/j.buildenv.2020.107460
Received 10 August 2020; Received in revised form 26 October 2020; Accepted 8 November 2020
Available online 12 November 2020

permeability tend to lead to high moisture contents in the masonry. Therefore, the response of masonry walls to internal insulation may be very different depending on the moisture transport properties of the rendering. Künzel [19] recommended improving the rain protection measures at the facade. As an active control means, local heating is a method that allows increasing the temperature at the wooden beam-end. Wegerer and Bednar [20] used a metal sheet, driven into the construction at the joint between the wooden beam and the surrounding masonry, to heat the wooden beam-end. The higher temperature at the wooden beam-end will increase the drying potential and lead to lower moisture content levels, thus lowering moisture risks for the wooden beam-end.

Moisture and heat transport in masonry walls with wooden beams is, in reality, a three-dimensional problem [21,22]. However, many numerical studies use only two-dimensional hygrothermal models to study the moisture risk of wooden beam-ends in internally insulated masonry. For example, Guizzardi et al. [3] analysed such risk of biodeterioration with WUFI 2D, a two-dimensional hygrothermal model. Johansson et al. [23] used also WUFI 2D for investigating the hygrothermal performance of a similar assembly internally insulated with vacuum insulation panels. Harrestrup and Svendsen [4] used the 2D model Delphin to investigate the effect of three different insulation strategies on the risk of mould growth in the wooden beam-ends. In a 2D model, the wooden beam is assumed to have the same width as the wall envelope. However, in reality, the width of wooden beam is much smaller compared to that of the wall envelope. The much larger width of wooden beam in the 2D model could have influence on moisture and heat transport in the wall envelope as the hygrothermal properties of wood is quite different from masonry. It is still an open question whether a simplified two-dimensional numerical model can represent accurately the hygrothermal conditions as modeled in 3D.

The objective of this paper is to study moisture risk of wooden beam-ends embedded in internally insulated masonry walls with 2D and 3D hygrothermal modelling. A hygrothermal model that can consider both moisture and heat transport in building envelopes is developed. A 2D model with a simplified distribution of bricks and mortar joints is built and compared with a detailed 2D model. Based on the results of the simplified 2D model, a 3D model is developed. The influence of varying materials, i.e. render type and vapour control strategy, or of active local heating on 2D and 3D modelling is analysed. The difference in relative humidity, moisture content, temperature and mould index between 2D and 3D modelling is compared.

2. Modelling

2.1. Methodology

A typical historical masonry wall structure of Switzerland consists of 2–4 brick wythes, finished on the exterior with exterior rendering and on the interior with plaster, and receives wood floor members. The geometry of the 2D model with a detailed configuration of bricks and mortar joints is shown in Fig. 1a. The 2D model comprises, from exterior to interior, an exterior render, a masonry wall (three wythes of clay brick) and an original interior plaster. As a mode of inside retrofit, we select to add an aerogel-based insulation layer and a new interior plaster layer. Aerogel-based insulations are characterized by a low thermal conductivity and due to the ease in applying the render by spraying on uneven surfaces, it is an appropriate inside insulation method for heritage buildings. We consider here a mix of aerogel particles and plaster binder. The minimized inner space loss as a result of using a highly-insulating plaster, such as the aerogel-based insulation, is an attractive feature, especially for buildings in cities in Switzerland. We select a main beam, as the inserted wood member, that measures 30 cm high by 20 cm wide. A 1-cm thick air gap lies in front of the wooden beam-end. The air gap prevents direct contact between the wooden beam and the masonry and functions as a capillary break. The U value of the non-insulated wall envelope is 1.20 (W/m^2/K). In Switzerland, it is required by the SIA-Norm 380/1 that the U value for wall envelopes after energy renovation should be smaller than 0.25 W/m^{2}K. However, for internal thermal insulation projects, an exception is allowed. Considering energy saving and space loss, the thickness of aerogel insulating plaster is selected as 6 cm. Thus, after internal energy retrofitting, the U value of the wall envelope decreases to 0.31 W/m^{2}K.

Masonry is a system made of a large number of bricks joined by

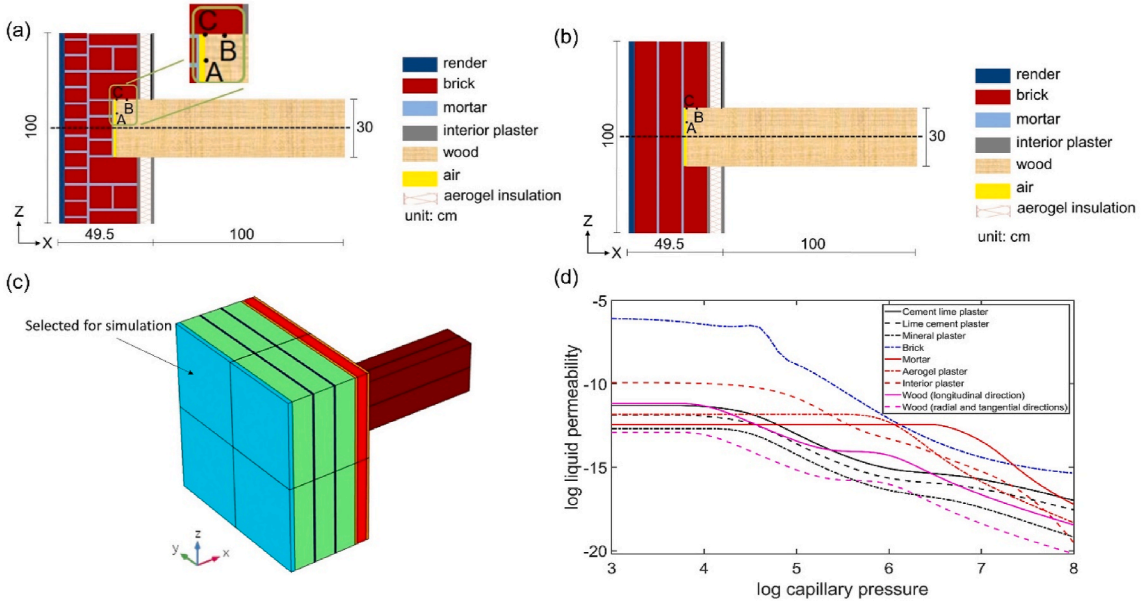

Fig. 1. (a) Two-dimensional schematic representation of computational domain for a wooden beam embedded in an internally insulated masonry wall, using the detailed description of the masonry configuration; (b) Two-dimensional schematic representation of computational domain for a wooden beam embedded in an internally insulated masonry wall, using a simplification of the masonry configuration; (c) Three-dimensional schematic representation of computational domain for a wooden beam in an internally insulated masonry wall, where due to symmetry only one quarter of the geometry of the 3D model is retained for modelling; (d) Liquid permeability of the materials.

mortar. From a modelling point of view, it is hardly feasible and probably not relevant to model all bricks and mortar joints of a masonry wall in 3D, since such approach would yield large computational meshes and high computational costs. We thus simplify the masonry in a 2D model built with simplified vertical layers of bricks and mortar joints, as horizontal mortar joints are discarded. The simplified 2D model of this wall is shown in Fig. 1b. The main moisture flow direction is in horizontal direction. Therefore, the vertical mortar joints are kept since they may act as barriers to moisture flow. The simulated results from the 3D and 2D models are compared and discussed. The 3D model follows the geometry of the simplified 2D model, as shown in Fig. 1c. In 3D, the width of the masonry wall is 100 cm and the width of the wooden beam is 20 cm. Considering the symmetry of the geometry, only the top half of the 2D geometry, i.e. above the dashed line in Fig. 1a and b is simulated. For the 3D model, a quarter of the geometry of the 3D model is simulated owing to the symmetry of the geometry (Fig. 1c).

We monitor relative humidity, temperature and moisture content at three locations denoted A, B and C as shown in Fig. 1a and b. Point A is located next to the air gap in front of the wooden beam. Point B is located on the top of the wooden beam in contact with the masonry wall. Point C is located at the corner of the beam. In the 3D simulations, these three locations are considered in two longitudinal cross section of the wood beam: at central and at the edge of the wood beam, thus for a total of 6 locations.

We study here the influence of the render type, the vapour permeability of the insulation system and the presence of heating at the end of the wood beam on the hygrothermal performance considering the 2D and 3D models. Three types of renders with different water uptake capacities are considered. Regarding the vapour permeability of the insulation system, we consider both a vapour-open and a vapour-tight interior insulation systems.

2.2. Material properties

Three types of exterior render are considered, namely cement lime plaster, lime cement plaster and mineral plaster, which are used to study the influence of the level of rain protection provided by the render on the moisture-related damage risks of wooden beam-ends embedded in internally insulated masonry walls. The cement lime plaster shows the highest liquid permeability, followed by the lime cement plaster and the mineral plaster shows the lowest liquid permeability and thus the highest rain protection (Fig. 1d). The vapour resistance factor of the renders is similar ranging between 19 and 25 (Table 1). The material properties of brick and interior plaster are taken from Hagentoft et al. [24]. The material properties of mortar are taken from Guizzardi [25]. No hydraulic interface resistance is considered between brick and mortar. The material properties of aerogel plaster are taken from Guizzardi [25]. The wood species of the beam is spruce. Its material properties are obtained from the WUFI database [26]. The wood is considered orthotropic, with the longitudinal direction along the beam orientation. Vapour permeability and thermal conductivity along the longitudinal direction are different from those of the transverse, i.e. radial and tangential directions (Table 1). The material properties of the 1-cm thick air layer are taken from the WUFI database [26]. The effective material parameters of air consider total heat transport due to heat conduction, free convection and radiative transport and total vapour transport due to diffusion and free convection in an unventilated air layer between non-metallic surfaces. No liquid water transport may occur in the air layer (liquid permeability set to 0 (s)).

The capillary pressure curve of the building materials is described using a multimodal function of the van Genuchten model [27,28]:

$$w = w_{cap} \sum_{i=1}^{N} \frac{k_i}{\left(1 + a_i \cdot \mathrm{abs}(p_c)^{n_i}\right)^{m_i}} \quad (1)$$

where w_{cap} is the capillary saturation moisture content (kg/m^3); p_c is the capillary pressure (Pa); k is the weighting parameter, a, m and n are fitting parameters where $m = 1\text{-}1/n$; N is the modal number and i is the counter.

The thermal conductivity of the building materials is given by:

$$\lambda = \lambda_{dry} + a \cdot w \quad (2)$$

where $\lambda_{dry}$is the dry thermal conductivity (W/mK), a is a parameter describing the influence of moisture content on thermal conductivity, w is the moisture content (kg/m^3).

The interior insulation with aerogel insulation is very vapour-open.

Table 1
Properties of the building materials.

	Density (kg/m^3)	Heat capacity (J/kg/K)	Capillary moisture content (kg/m^3)	Water absorption coefficient (kg/m^2/h$^{0.5}$)	Moisture retention parameters				Water vapour resistance factor, dry (mu_{dry})	Thermal conductivity	
					N	k	a	n		λ_{dry} (W/mK)	a
Cement lime plaster	1900	850	210	0.47	3	0.21	5.0e-5	1.6	19	0.8	3.4e-3
						0.36	2.6e-5	1.2			
						0.43	2.0e-7	1.4			
Lime cement plaster	1900	850	210	0.26	3	0.21	5.0e-5	1.6	19	0.8	3.4e-3
						0.36	2.6e-5	1.2			
						0.43	2.0e-7	1.4			
Mineral plaster	1900	850	210	0.14	3	0.21	5.0e-5	1.6	25	0.8	3.4e-3
						0.36	2.6e-5	1.2			
						0.43	2.0e-7	1.4			
Brick	1600	1000	373.5	202.8	2	0.46	4.8e-5	1.5	7.5	0.68	0.0
						0.54	2.0e-5	3.8			
Mortar	1623	850	146	1.51	2	0.5	7.0e-8	3.0	19	0.63	0.0
						0.5	2.0e-7	2.2			
Aerogel plaster	200	1000	400	/	2	0.8	6.9e-7	2.3	4	0.025	6.0e-4
						0.2	1.8e-6	2.0			
Interior plaster	79	790	209	/	1	1.0	2.0e-6	1.27	3	0.2	4.5e-3
Air layer	1.3	1000	0.017	/	/	/	/	/	0.73	0.071	0.0
Wood (longitudinal direction)	455	1500	600	/	3	0.25	9.0e-7	2.5	4.3	0.23	6.6e-4
						0.4	7.0e-7	1.42			
						0.35	9.0e-5	2.0			
Wood (radial and tangential directions)	455	1500	600	/	3	0.25	9.0e-7	2.5	130	0.09	2.6e-4
						0.4	7.0e-7	1.42			
						0.35	9.0e-5	2.0			

Moisture in the wall envelopes can dry both to the outside and inside environments. In order to also compare the hygrothermal performance of 2D and 3D models in vapour-tight insulation system, a paint layer with vapour diffusion resistance of 10 m is added on the inside surface of aerogel insulation layer. This would also be the equivalent of adding a vapour barrier to the inside surface of the aerogel insulation layer. This case is considered since the render may be painted in future by a more vapour-tight paint.

2.3. Governing equations for moisture and heat transport

The three-dimensional governing equations for coupled moisture and heat transport in the building wall assemblies are [29]:

Conservation of moisture:

$$\frac{\partial w}{\partial p_c}\frac{\partial p_c}{\partial t}+\frac{\partial}{\partial x_i}(g_l+g_v)=0 \tag{3}$$

with liquid flow:

$$g_l=-KL_{i,j}(p_c)\frac{\partial p_c}{\partial x_j} \tag{4}$$

and vapour flow:

$$g_v=-\delta_{i,j}(w)\cdot\frac{p_v}{\rho_l\cdot R_v\cdot T}\frac{\partial p_c}{\partial x_j}-\delta_{i,j}(w)\cdot\frac{p_v}{\rho_l\cdot R_v\cdot T^2}(\rho_l\cdot L_v)\cdot\frac{\partial T}{\partial x_j} \tag{5}$$

Conservation of heat:

$$(c_0\cdot\rho_0+c_l\cdot w)\cdot\frac{\partial T}{\partial t}+\nabla\cdot\left(c_l\cdot\left(T-T_{ref}\right)\cdot g_l+\left(c_v\cdot\left(T-T_{ref}\right)+L_v\right)\cdot g_v\right)=-\frac{\partial}{\partial x_i}\left(\lambda_{i,j}(w)\frac{\partial T}{\partial x_j}\right) \tag{6}$$

where w is the moisture content (kg/m^3), p_c is the capillary pressure (Pa), g_l and g_v are the liquid and vapour flows (kg/m^{2}s), $i, j = 1, 2, 3$ ($x_1 = x$, $x_2 = y$, $x_3 = z$), $KL_{i,j}(p_c)$ is the liquid permeability (s), $\delta_{i,j}(w)$ is the water vapour permeability (s), p_v is the vapour pressure (Pa), ρ_l is the density of water (kg/m^3), R_v is the gas constant of water (J/kg K), T is the temperature (K), c_0 is the specific heat capacity of solids (J/kg K), c_l is the specific heat capacity of water (J/kg K), c_v is the specific heat capacity of vapour (J/kg K), ρ_0 is the density of solid (kg/m^3), T_{ref} is the reference temperature (273.15 K), L_v is the latent heat of vapourization (J/kg), $\lambda_{i,j}(w)$ is the thermal conductivity (W/mK).

Assuming that the coordinate axes x, y and z are alined with the principal directions of the tensors of liquid permeability, water vapour permeability and thermal conductivity, equations (4) and (5) can be changed to:

$$g_l=-KL_{x,x}(p_c)\frac{\partial p_c}{\partial x}-KL_{y,y}(p_c)\frac{\partial p_c}{\partial y}-KL_{z,z}(p_c)\frac{\partial p_c}{\partial z} \tag{7}$$

$$\begin{aligned}g_v=&-\frac{p_v}{\rho_l\cdot R_v\cdot T}\left(\delta_{x,x}(w)\frac{\partial p_c}{\partial x}+\delta_{y,y}(w)\frac{\partial p_c}{\partial y}+\delta_{z,z}(w)\frac{\partial p_c}{\partial z}\right)\\&-\frac{p_v}{\rho_l\cdot R_v\cdot T^2}(\rho_l\cdot L_v)\cdot\left(\delta_{x,x}(w)\frac{\partial T}{\partial x}+\delta_{y,y}(w)\frac{\partial T}{\partial y}+\delta_{z,z}(w)\frac{\partial T}{\partial z}\right)\end{aligned} \tag{8}$$

The governing moisture and heat transport equations (3) and (6) can be changed to

$$\begin{aligned}&\frac{\partial w}{\partial p_c}\frac{\partial p_c}{\partial t}-\frac{\partial}{\partial x}\left(KL_{x,x}(p_c)\frac{\partial p_c}{\partial x}\right)-\frac{\partial}{\partial y}\left(KL_{y,y}(p_c)\frac{\partial p_c}{\partial y}\right)-\frac{\partial}{\partial z}\left(KL_{z,z}(p_c)\frac{\partial p_c}{\partial z}\right)\\&-\frac{p_v}{\rho_l\cdot R_v\cdot T}\left(\frac{\partial}{\partial x}\left(\delta_{x,x}(w)\frac{\partial p_c}{\partial x}\right)+\frac{\partial}{\partial y}\left(\delta_{y,y}(w)\frac{\partial p_c}{\partial y}\right)+\frac{\partial}{\partial z}\left(\delta_{z,z}(w)\frac{\partial p_c}{\partial z}\right)\right)\\&-\frac{p_v}{\rho_l\cdot R_v\cdot T^2}(\rho_l\cdot L_v)\cdot\left(\frac{\partial}{\partial x}\left(\delta_{x,x}(w)\frac{\partial T}{\partial x}\right)+\frac{\partial}{\partial y}\left(\delta_{y,y}(w)\frac{\partial T}{\partial y}\right)+\frac{\partial}{\partial z}\left(\delta_{z,z}(w)\frac{\partial T}{\partial z}\right)\right)=0\end{aligned} \tag{9}$$

$$\begin{aligned}&(c_0\cdot\rho_0+c_l\cdot w)\cdot\tfrac{\partial T}{\partial t}+\nabla\cdot\left(c_l\cdot\left(T-T_{ref}\right)\cdot g_l+\left(c_v\cdot\left(T-T_{ref}\right)+L_v\right)\cdot g_v\right)\\&-\frac{\partial}{\partial x}\left(\lambda_{x,x}(w)\frac{\partial T}{\partial x}\right)-\frac{\partial}{\partial y}\left(\lambda_{y,y}(w)\frac{\partial T}{\partial y}\right)-\frac{\partial}{\partial z}\left(\lambda_{z,z}(w)\frac{\partial T}{\partial z}\right)\end{aligned} \tag{10}$$

For two-dimensional modelling, the properties in the y-direction are not used. The coupled heat and mass transfer model was validated with HAMSTAD benchmark 4 and 5 [24].

2.4. Initial and boundary conditions

The hygrothermal performance analysis is based on the moisture reference year 1999 for Zurich [30]. This year is a moist year with a return period of 10 years, selected over the period 1981–2010. The selected wall orientation is 240° from north (WSW), which shows the highest risk for moisture-related problems. The exterior conditions consist of hourly values of outdoor air temperature, relative humidity, wind speed, wind direction, solar radiation and horizontal precipitation, as given by the meteorological data from the MeteoSwiss meteorological station for Zürich. The exterior convective heat transfer coefficient is calculated according to the European standard EN15026 [31]. The exterior mass transfer coefficient is related to the exterior convective heat transfer by the use of the Lewis analogy. The short-wave and long-wave absorptivity of the exterior wall surface are 0.7 and 0.93, respectively. The calculation of net radiation at the exterior wall surface follows the method used in Janssen et al. [29]. The wind-driven rain load on the wall surface is calculated according to ASHRAE Standard 160 - Criteria for Moisture Control Design Analysis in Buildings [32]. According to Künzel and Kiessl [33], 70% of the wind-driven rain hitting the façade remains pinned in place; the rest splashes off the surface. The interior conditions are determined according to the European standard EN15026 [31], in which the indoor air temperature and relative humidity depend linearly on the outdoor temperature. The building components have an initial temperature of 20.0 °C and a relative humidity of 60%. The simulation is started from October 1st and repeated for 8 years. The results of the 8th year, which are found to be independent of the initial conditions, are used for the present analysis.

3. Results

We present the results of the investigation in three parts. First, considering the 2D approaches, we look at the consequences of simplifying the configuration of the masonry. Then, we look at the impact of modelling the beam 3-dimensional versus 2-dimensional for different cases obtained by varying the material properties. Third, we investigate the effect of active local heating on the assembly hygrothermal performance with the 2D and 3D models.

3.1. Comparison of results between detailed and simplified 2D models

The simulated results of the 2D detailed and simplified models are given for the three selected positions at the wooden beam for different renderings. Although the distribution of bricks and mortar joints is different between the detailed and simplified 2D models, the relative humidity profiles are very close between these two models (Fig. 2). For the render of cement lime plaster and mineral plaster, the largest difference in relative humidity between the two models is less than 0.01. For the render of lime cement plaster, the largest difference in relative humidity is less than 0.02. For all the three renders, the relative humidity is almost the same between the two models at Point C. In general, the relative humidity in the simplified 2D model is slightly higher during the cold period, whereas it is slightly lower during the warm period. The simulated temperature at the three positions in the wooden beam for the detailed and simplified 2D geometries are compared in Fig. 3. The difference in temperature between different points is for all cases very small, the largest difference in temperature being less than 0.1°C. The difference in moisture content is larger for the wall envelopes with the render of cement lime plaster than the other two renders (Fig. 4). For the envelopes with the render of cement lime plaster, the difference in moisture content is larger at point C than at points A and B. The maximum difference in moisture content is 0.023 kg/kg at point C in the case of vapour-tight insulation system. For the renders with lime cement plaster and mineral plaster, the difference in moisture content is very small and the largest difference in moisture content is only 0.009 kg/kg. As the moisture-related damage occurs in the cold period, the result from the simplified 2D model will be slightly conservative compared to the detailed model.

The reasons for higher moisture content and relative humidity in the simplified model versus the detailed one at points A, B and C regardless of the render type are explained as follows. The capillary moisture content of the mortar is much smaller than that of brick (Table 1). The number of mortar joints in the simplified model is much smaller than that in the detailed one, resulting in less capacity to store moisture in the masonry. As the moisture supply by rain is the same for both models, the fact that less moisture is stored in the masonry in the simplified 2D model results in more moisture that can be stored in the wooden beam. Consequently, the points A, B and C in the simplified model show higher moisture content. When the render has a larger liquid permeability such as the cement lime plaster, the moisture content and relative humidity in the wall are at higher level. Consequently, the differences in moisture content and relative humidity between the simplified model and the detailed model are larger. In reverse, the renders with lower liquid permeability such as the lime cement plaster and mineral plaster, yields lower levels of moisture content and relative humidity and smaller differences in moisture content and relative humidity between the models are observed. As the thermal properties of brick and mortar are very close to each other, the difference in temperature between the two models is very small. Considering the small difference in relative humidity, temperature and moisture content between the simplified and detailed 2D models, simplification of the detailed distribution of brick and mortar joint is reasonable and justified and the simplified 2D model is retained as a good model for the actual masonry configuration.

Looking at the temperature at the three points in the wall assemblies with different renders, the influence of the render type is very small as the cases with different renders have almost all the same temperature profiles (Fig. 3). The relative humidity and moisture content in the wooden beam-end is, however, strongly affected by the type of exterior render. The render with a larger liquid permeability, namely cement lime plaster, leads to higher values in relative humidity and moisture content in the wooden beam end. We note that for this render, the relative humidity and moisture content are much higher in the case with vapour-tight insulation than the case with vapour-open insulation. For example, for the simplified model, the relative humidity (RH) at point B in the case with vapour-tight insulation varies between 0.89 and 0.95, while in the case with vapour-open insulation RH varies between 0.77 and 0.90 (Fig. 2). The moisture content at point B varies between 0.20 -

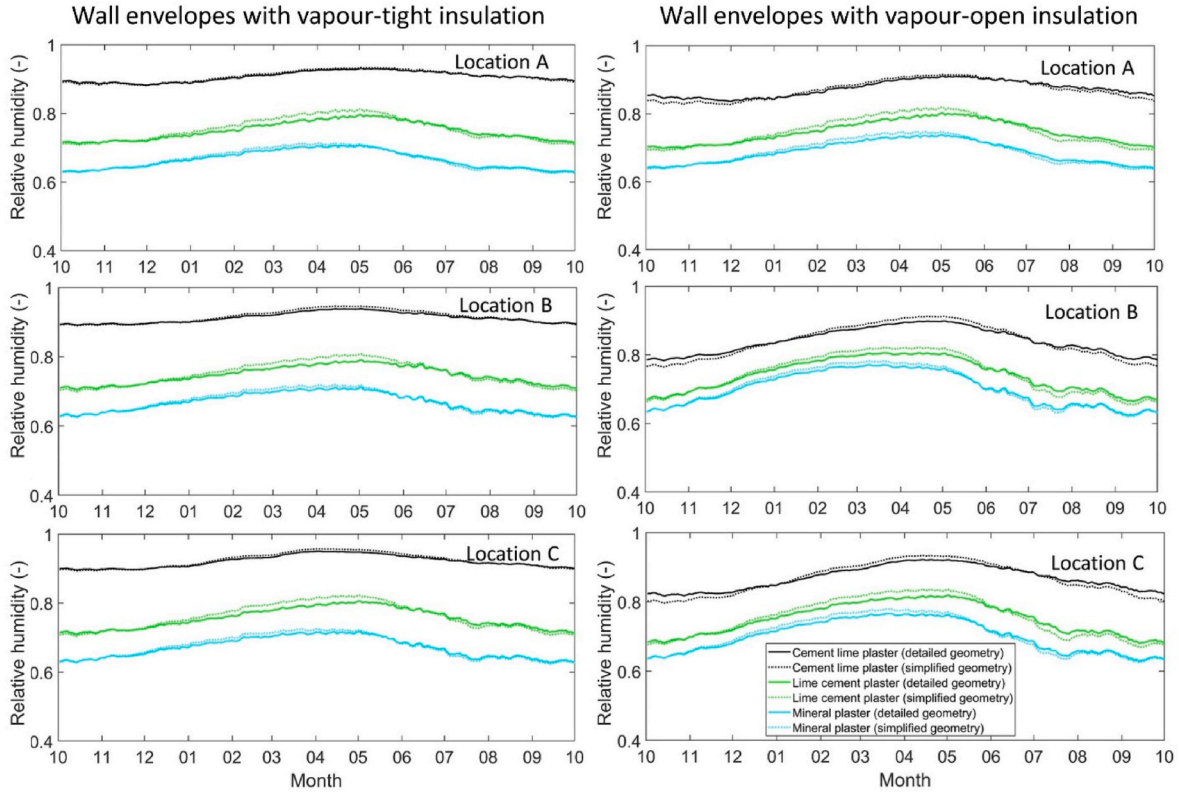

Fig. 2. Relative humidity at points A, B and C in the detailed and simplified 2D geometries using different renderings.

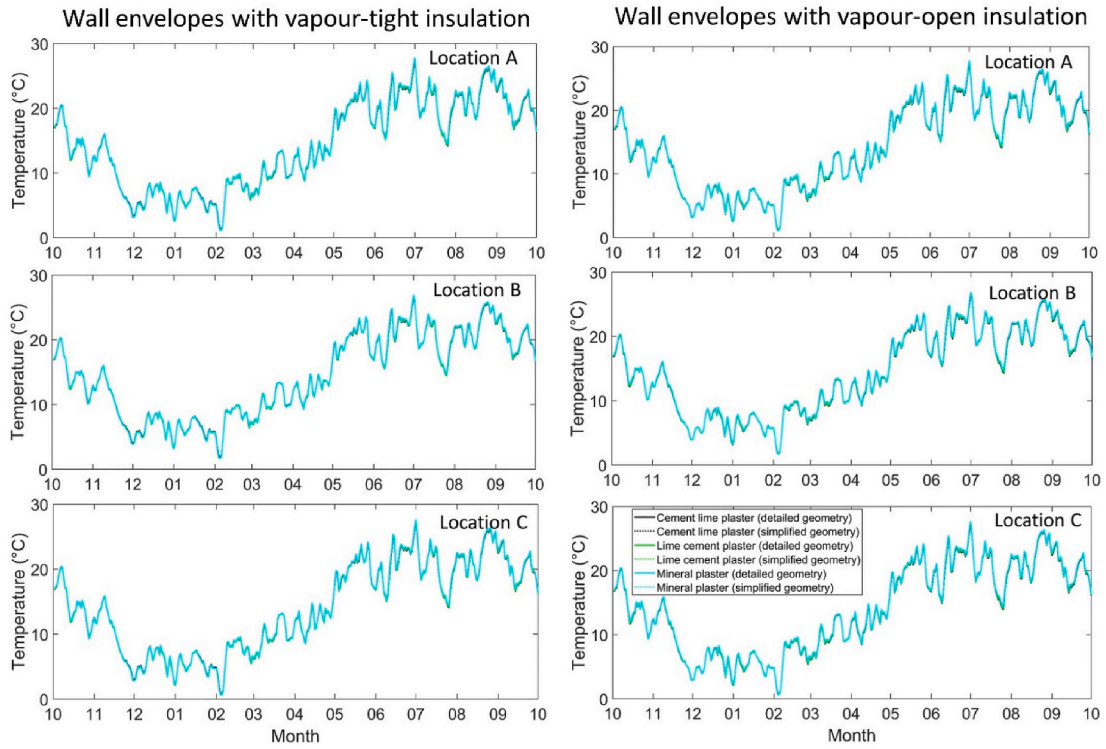

Fig. 3. Temperature at points A, B and C in the detailed and simplified 2D geometries.

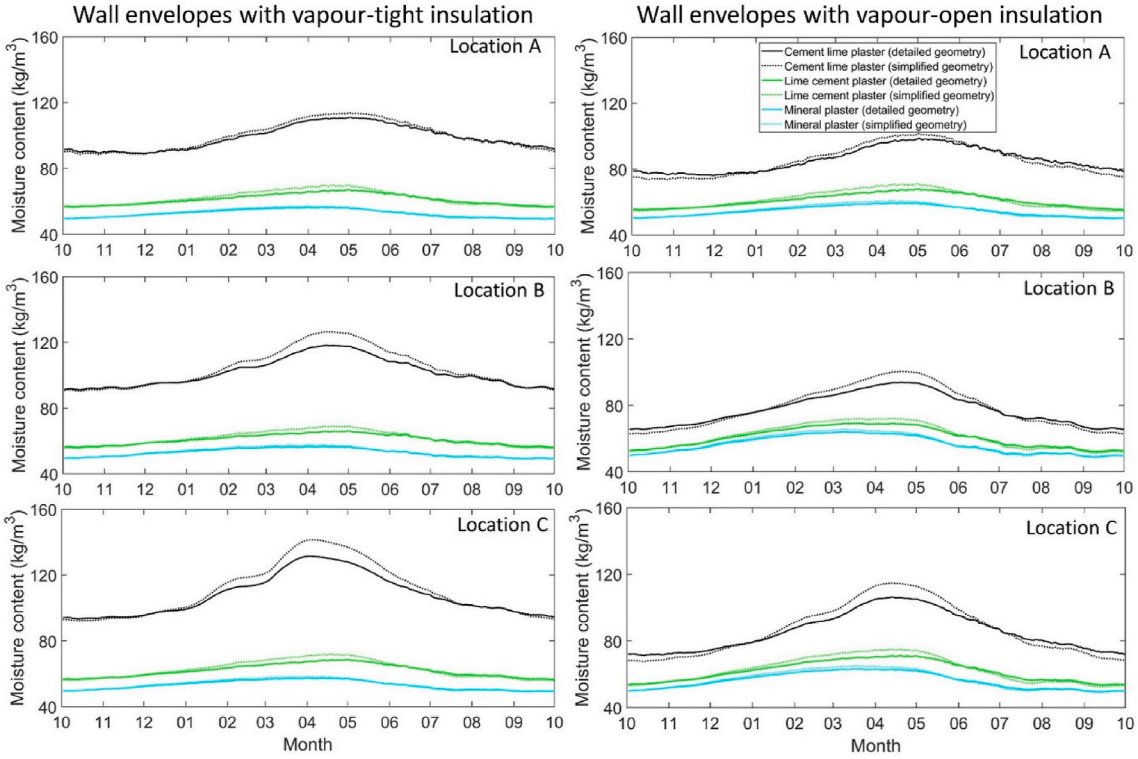

Fig. 4. Moisture content at points A, B and C in the detailed and simplified 2D geometries using different renderings.

0.28 and 0.14–0.22 kg/kg for the vapour-tight and vapour-open insulation, respectively (Fig. 4).

The 2D relative humidity distribution is compared between the wall envelopes with vapour-open and vapour-tight insulations in Fig. 5a. Relative humidity is the largest at the upper left corner of the wooden beam for both cases. The contour lines indicate the edge of the wooden beam-end shows larger relative humidity than the other part of the wooden beam-end. The 2D relative humidity distribution also shows higher relative humidities in the wooden beam-end in the case with vapour-tight insulation than the case with vapour-open insulation. For

the wall envelope with the render of lime cement plaster and mineral plaster (lower liquid permeability), the difference in relative humidity between the wall envelopes with vapour-open and vapour-tight insulation is much smaller (Fig. 2). Compared to the wall envelopes with vapour-open insulation, the wall envelopes with vapour-tight insulation show smaller fluctuations in RH, which is due to lower drying ability to the indoor environment. To illustrate this lower drying, we report the total vapour flux calculated along the whole interior surface in the simplified 2D model for wall envelope with the render of cement lime plaster retrofitted with vapour-open and vapour-tight insulations, see Fig. 5b. A negative value indicates drying flux to the indoor environment. The drying vapour flux to the indoor environment is very large from April to September for the wall envelope with vapour-open insulation. By comparison, the drying flux is very small for the wall envelope with vapour-tight insulation in this period.

3.2. Comparison of results between 2D and 3D models

As the wood beam embedded in the masonry has a width, we consider the real width of the wooden beam of 20 cm in the 3D model. In contrast, in 2D the wooden beam spans over the total width of the wall. Although wood has a rather low thermal conductivity, the wooden beam is a thermal bridge in the internally insulated masonry wall due to much lower thermal conductivity of the insulation layer. The thermal bridge effect leads to higher temperature and thus lower relative humidity in the wooden beam than in the masonry wall. Due to the higher heat flux

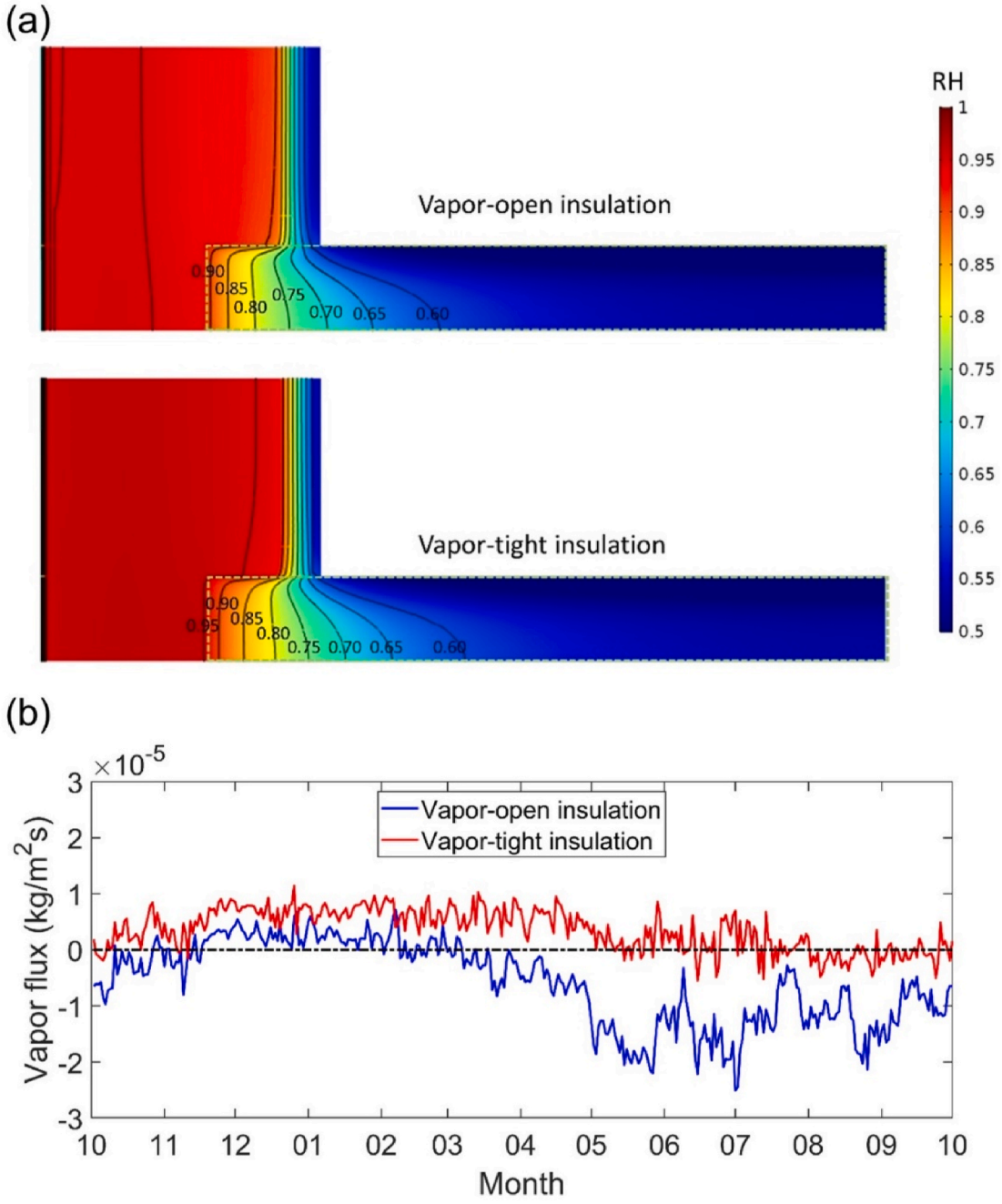

Fig. 5. (a) Relative humidity distribution on 1st April in the simplified 2D model for wall envelope with the render of cement lime plaster retrofitted with vapour-open and vapour-tight insulation (the dashed box indicates the location of the wooden beam); (b) Total vapour flux across interior boundary of the simplified 2D model for wall envelope with the render of cement lime plaster retrofitted with vapour-open and vapour-tight insulations.

in the beam, the central cross section of the wooden beam embedded in the masonry wall will be the warmest cross section of the wooden beam during the winter period, while the edge cross section in contact with masonry wall will be the coldest one. Similarly, the central cross section will have the lowest relative humidity whereas the edge cross section will have the highest one during the winter period. For example, Fig. 6 shows relative humidity distribution on the 1st of April in the 3D model for the wall envelope with the render of mineral plaster and vapour-open insulation. In the wooden part at the outside of the insulation (region I), the relative humidities in the wooden beam are smaller than the masonry above. At the surface of the wooden beam-end, the edge part in contact with the masonry wall shows higher relative humidities than the inner part, which is due to higher relative humidity in the surrounding masonry wall. At the surface of the wooden beam-end, the region closer to the central cross section shows lower relative humidity.

3.2.1. Comparison of relative humidity

For the interior insulation system with vapour-tight insulation, relative humidity in the 2D cross section is very similar to that in the 3D central cross section (Fig. 7). Relative humidity at the edge cross section of the 3D model is slightly larger than the RH at other cross sections. The difference in relative humidity between the 2D and 3D models is mostly very small ($\Delta RH < 0.014$) except at point A for the wall envelope with the render of cement lime plaster (highest liquid permeability), which is 0.033. Point A at the edge cross section of the 3D model is in contact with the masonry wall whereas point A in the 2D model and at the central cross section of the 3D model is separated from the masonry with the air gap. As the liquid permeability of cement lime plaster is relatively large allowing liquid water to ingress into the wall, moisture transport at point A at the edge cross section of the 3D model can be greatly influenced by liquid transport, which explains the higher relative humidity at point A. By comparison, point A in the 2D model and at the central cross section of the 3D model is separated from the masonry due to the presence of the air layer and is thus subjected to a lower relative humidity. As the interior insulation system is vapour-tight, drying towards the indoor environment is quite limited and thus the variation of relative humidity over the year remains small. Renders with larger liquid permeability lead to larger relative humidity values in the wall envelope. The relative humidity at points A, B and C varies around 0.9 for the wall envelope with cement lime plaster (large liquid permeability). By comparison, it varies around 0.7 for the wall envelope with mineral plaster (low liquid permeability).

For the vapour-open interior insulation system, the differences in relative humidity among different cross sections are larger (Fig. 8). The largest difference is in the wall envelope with mineral plaster (low liquid permeability). The difference in relative humidity between the 2D and 3D models for the wall envelope with mineral plaster can reach 0.06. In general, the fluctuation of relative humidity at the edge cross section of the 3D model is larger than at the central cross section, especially during the cold period. Relative humidity at point A at the central and edge cross sections is quite different depending on assembly composition whereas relative humidity at points B and C at the central and edge cross sections is very similar in all cases. For the wall envelope with the mineral plaster, relative humidity at point A is continuously below 0.8 in the 2D model while it can be slightly above 0.8 from February to June at the edge cross section in the 3D model.

3.2.2. Comparison of temperature

For wall envelopes with vapour-open and vapour-tight insulation, the temperature at the points A, B and C is very similar. We here only show the temperature in the winter period at points A, B and C in the 2D and 3D models for the wall envelopes with vapour-tight insulation (Fig. 9). In general, there are some differences in temperature between the 2D and 3D models. The temperature in the 2D cross section is the highest. The higher temperature in the 2D cross section is due to the larger width of the wooden beam and thus larger thermal bridge effect in

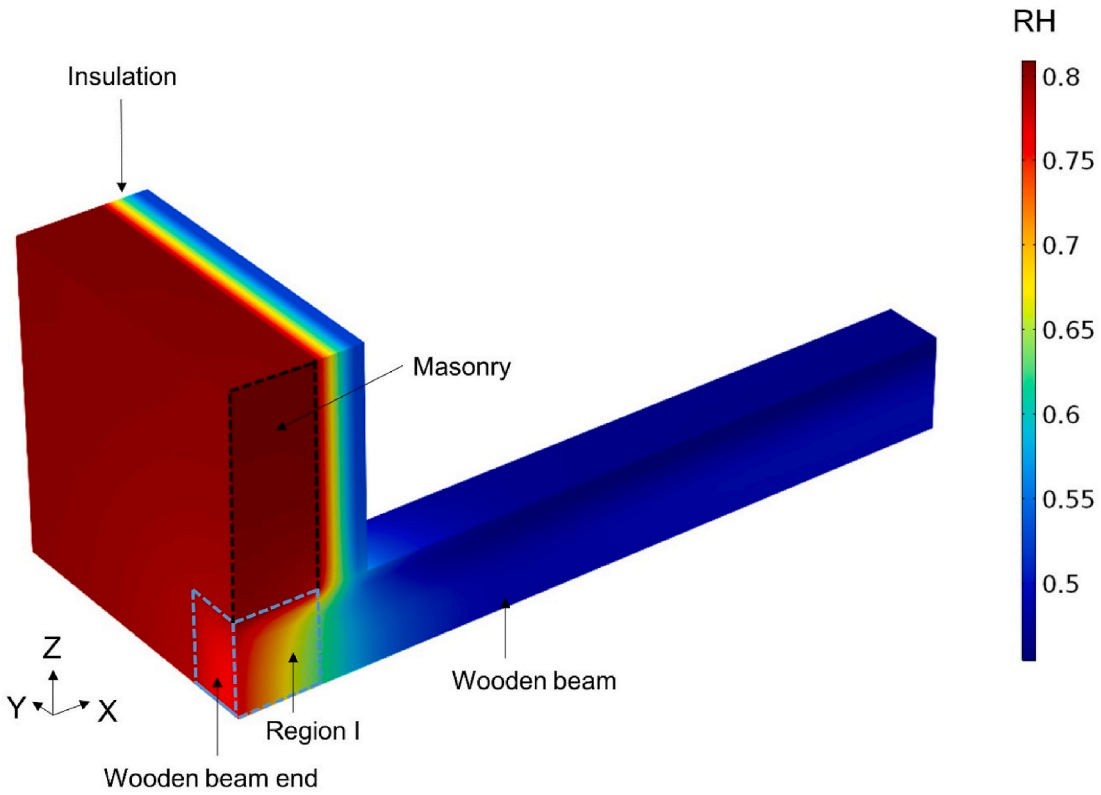

Fig. 6. Relative humidity distribution on 1st April in the 3D model for the wall envelope with the render of mineral plaster and vapour-open insulation. (The layers outside the wood beam-end surface are removed.)

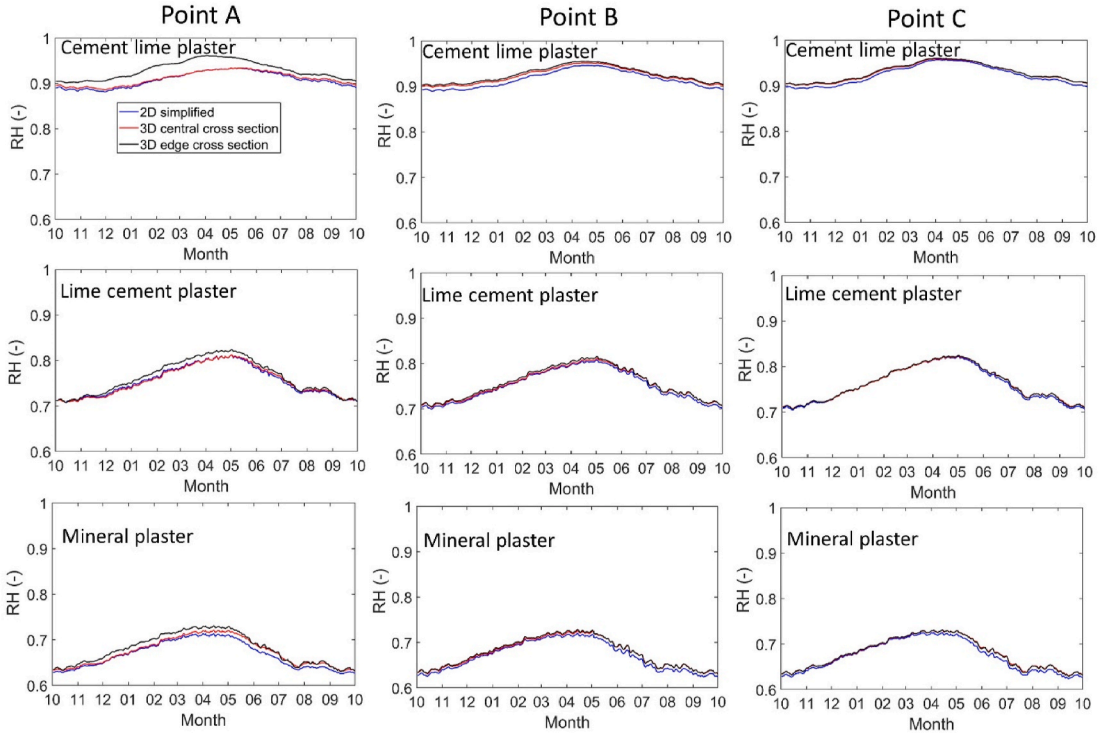

Fig. 7. Relative humidity at points A, B and C in the 2D model and central and edge cross section of the 3D model for wall envelopes with vapour-tight insulation.

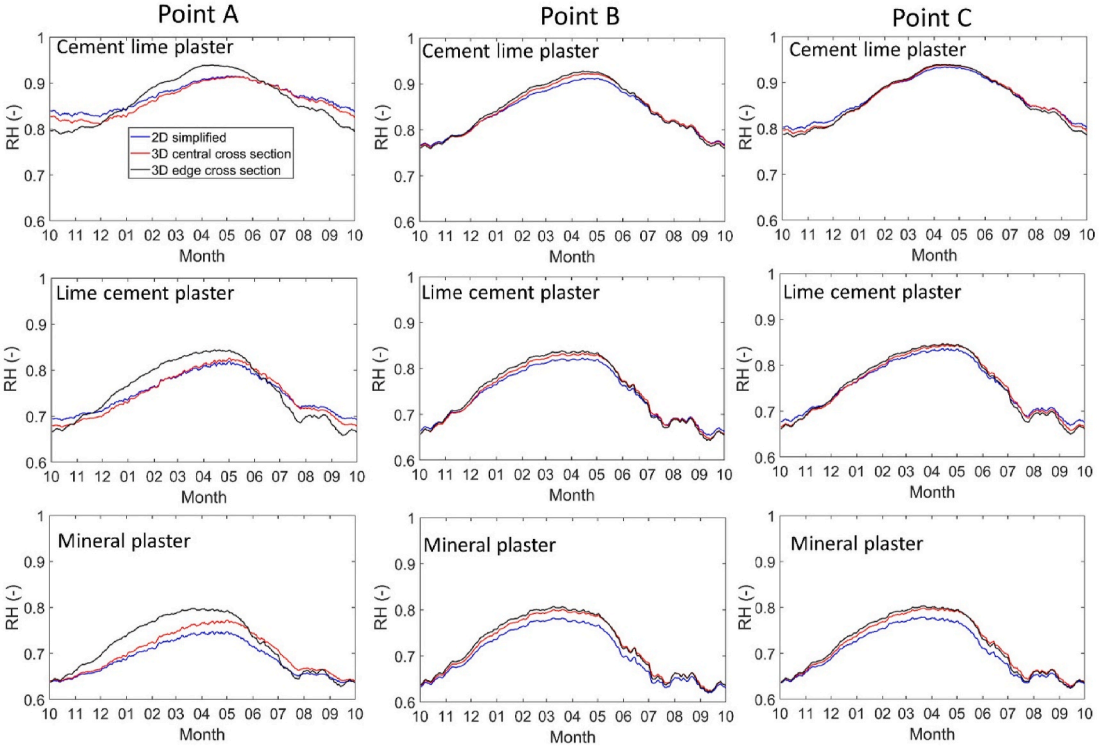

Fig. 8. Relative humidity at points A, B and C in the 2D model and central and edge cross section of the 3D model for wall envelopes with vapour-open insulation.

the 2D model. The largest temperature difference at points A, B and C between the 2D and 3D cross sections is 1.18°, while the smallest one is 0.02°. In the 3D model, the temperature in the central cross section is higher than that in the outermost cross section. The largest temperature difference at points A, B and C between the 3D central and 3D edge cross sections is 0.48°, while the smallest one is 0.02°.

It is found that the difference in temperature among wall envelopes with different renders is small. For example, the maximum temperature difference for the wall envelopes with different renders is 0.39° at point A. The difference is due to the different moisture content in the building materials, which affects the thermal conductivity of the building materials. However, in terms of temperature distribution, the difference

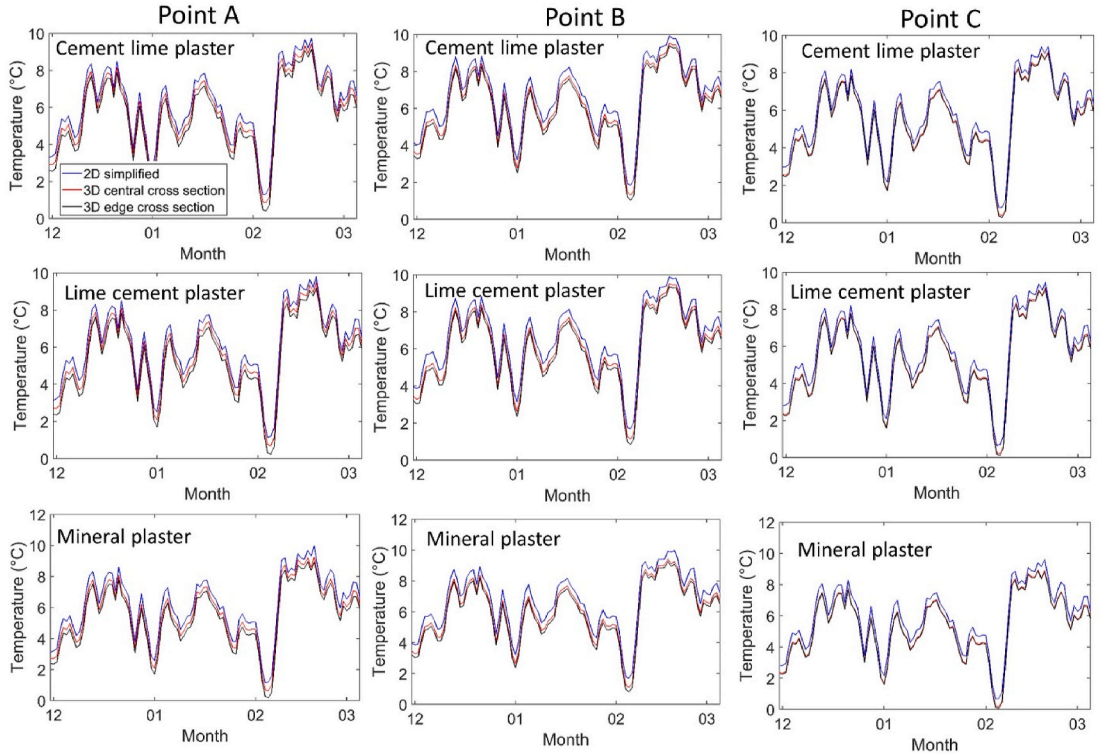

Fig. 9. Temperature at Points A, B and C in the 2D model and central and outermost cross section of the 3D model for wall envelopes with vapour-tight insulation in the winter period.

between the 2D and 3D models is overall quite small.

3.2.3. *Comparison of moisture content*

The differences in moisture content between the 2D and 3D models are similar as that in relative humidity , which is obvious as moisture content depends on relative humidity. For the interior insulation system with vapour-tight insulation, there is a very large difference in moisture content among the different cross sections at point A for the wall

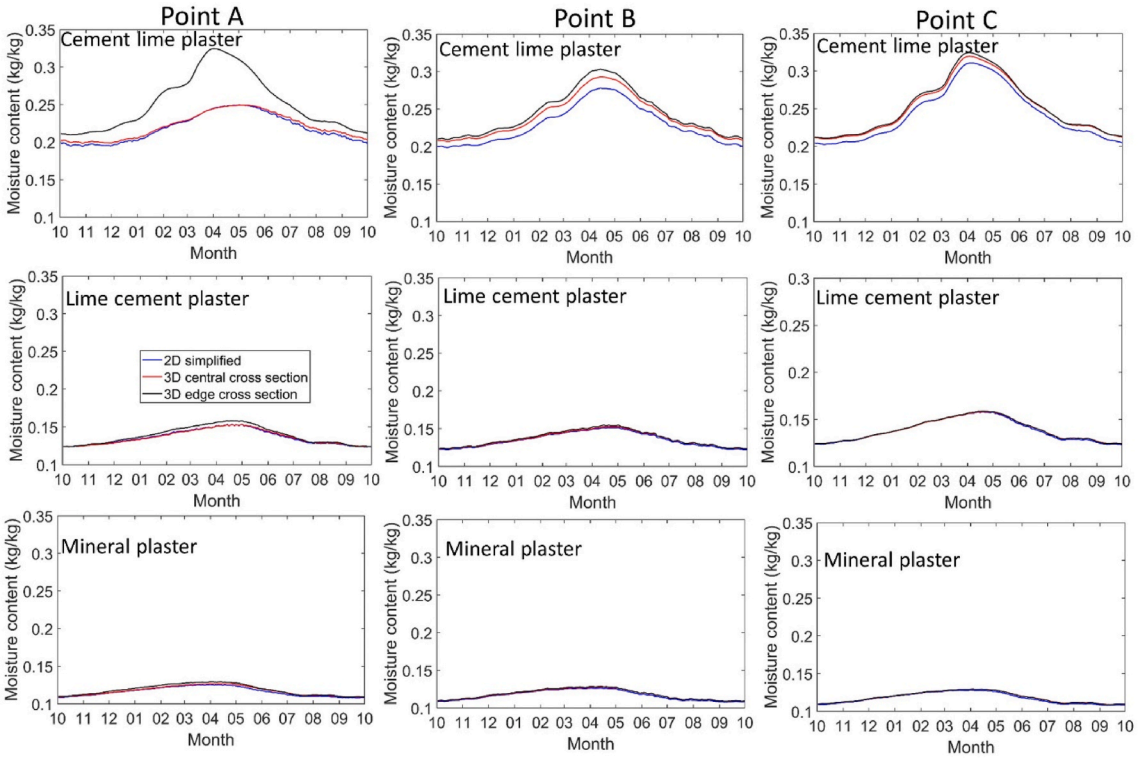

Fig. 10. Moisture content at points A, B and C in the 2D model and central and edge cross sections of the 3D model for wall envelopes with vapour-tight insulation.

envelope with the render of cement lime plaster (Fig. 10). However, the difference in moisture content among the different cross sections at point C, the location with the highest moisture content, is small. The difference in moisture content among the different cross sections at points A, B and C for the wall envelopes with the render of lime cement plaster and mineral plaster are very small.

For the vapour-open interior insulation system, the differences in moisture content among the different cross sections are mostly larger compared to the vapour-tight interior insulation system (Fig. 11). Points A, B and C at the edge cross sections mostly undergo larger moisture content than the points A, B and C at the central and 2D cross sections. Moisture content difference at point A between the difference cross sections is larger than at points B and C.

Comparing vapour-open and vapour-tight interior insulation systems, it is found that relative humidity and moisture content in the wooden beam in a vapour-tight interior system are smaller than in a vapour-open interior system, when the render has a low liquid permeability such as mineral plaster. By contrast, when the render has a high liquid permeability such as cement lime plaster, relative humidity and moisture content in a vapour-tight interior system are larger than in a vapour-open interior system. This result is similar to the results of one-dimensional parametric study from Zhou et al. [6]. When the liquid permeability of the render is large, moisture transport in the wall envelopes will significantly increase due to the liquid transport through the exterior render. Under such conditions, a vapour-open interior system provides additional drying potential towards the inside environment and leads to smaller moisture content in the wall. When liquid permeability of render is small, moisture transport will be mainly influenced by vapour transport. A vapour-tight insulation system will reduce vapour transport from the inside to the wall and eventually prevent condensation at the interface between masonry wall and interior insulation layer during cold periods and lead to a smaller relative humidity in the wall envelope.

3.2.4. Comparison of mould risk

The risk related to sustained exposure to moisture risk in the wall envelope is evaluated using the VTT Mould Index model [34] as indicator of risk. The VTT model is based on an empirical mould prediction model that considers the influence of temperature, relative humidity, surface, exposure time and dry periods. Fig. 12 show the maximum mould indices at the different wall envelopes. In general, for both vapour-open and vapour tight insulation systems, the moisture risk in the 2D model is slightly smaller than that in the 3D model. In the 3D model, the risk is higher at the edge cross section than at the central cross section. The difference in mould index between the 2D and 3D models is larger in the wall envelopes with vapour-open insulation than the wall envelopes with vapour-tight insulation.

For wall envelopes with render such as mineral plaster (low liquid permeability), the mould index at the wood beam-end is 0, because the relative humidity is continuously below the critical value of 0.8, and there is no risk of moisture problems after internal thermal insulation. For wall envelopes with render such as lime cement plaster (middle liquid permeability), the maximum mould index is below 1.0. In general, a mould index of 1 is regarded as tolerable since it means small amounts of mould on the wood. Therefore, the risk of moisture problems for these envelopes is acceptable. However, for envelopes with render such as cement lime plaster (high liquid permeability), the maximum mould index at the wood-beam end can reach 5. Such a mould index value means significant mould growth on the wood. The moisture risk in these wall envelopes is too high. Rain protection is thus needed for these wall envelopes to reduce moisture risk in the wooden beam.

Considering the small difference in mould indices, it is possible to replace a 3D model with a 2D model for evaluating the mould risk of wooden beam-ends embedded in internally insulated wall envelopes. In general, the difference in mould indices between the 2D and 3D models are relatively small and the mould risk at the different cross sections is in the same range. However, the 2D model will, in general, underestimate to some extent the mould risk compared to the 3D model. If more accurate relative humidity and moisture content in the wooden beam-end is needed, it might not be suitable to replace a 3D model with a 2D one for the envelopes with the render of cement lime plaster.

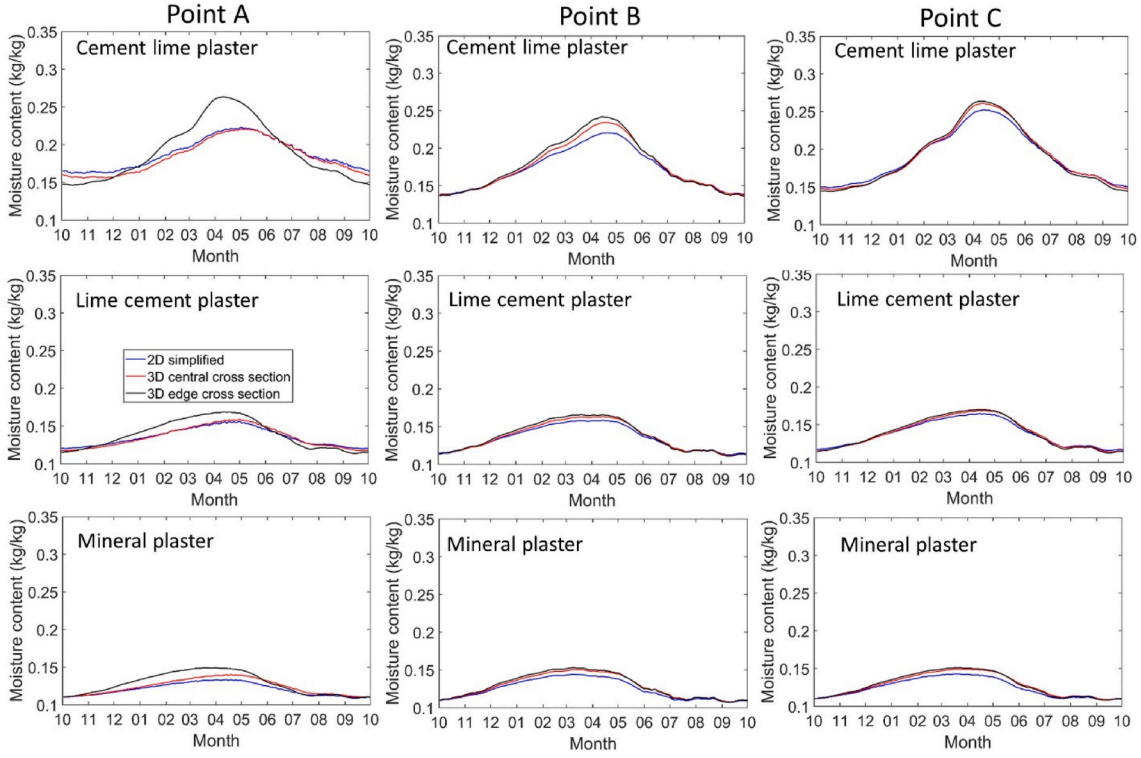

Fig. 11. Moisture content at points A, B and C in the 2D model and central and edge cross sections of the 3D model for wall envelopes with vapour-open insulation.

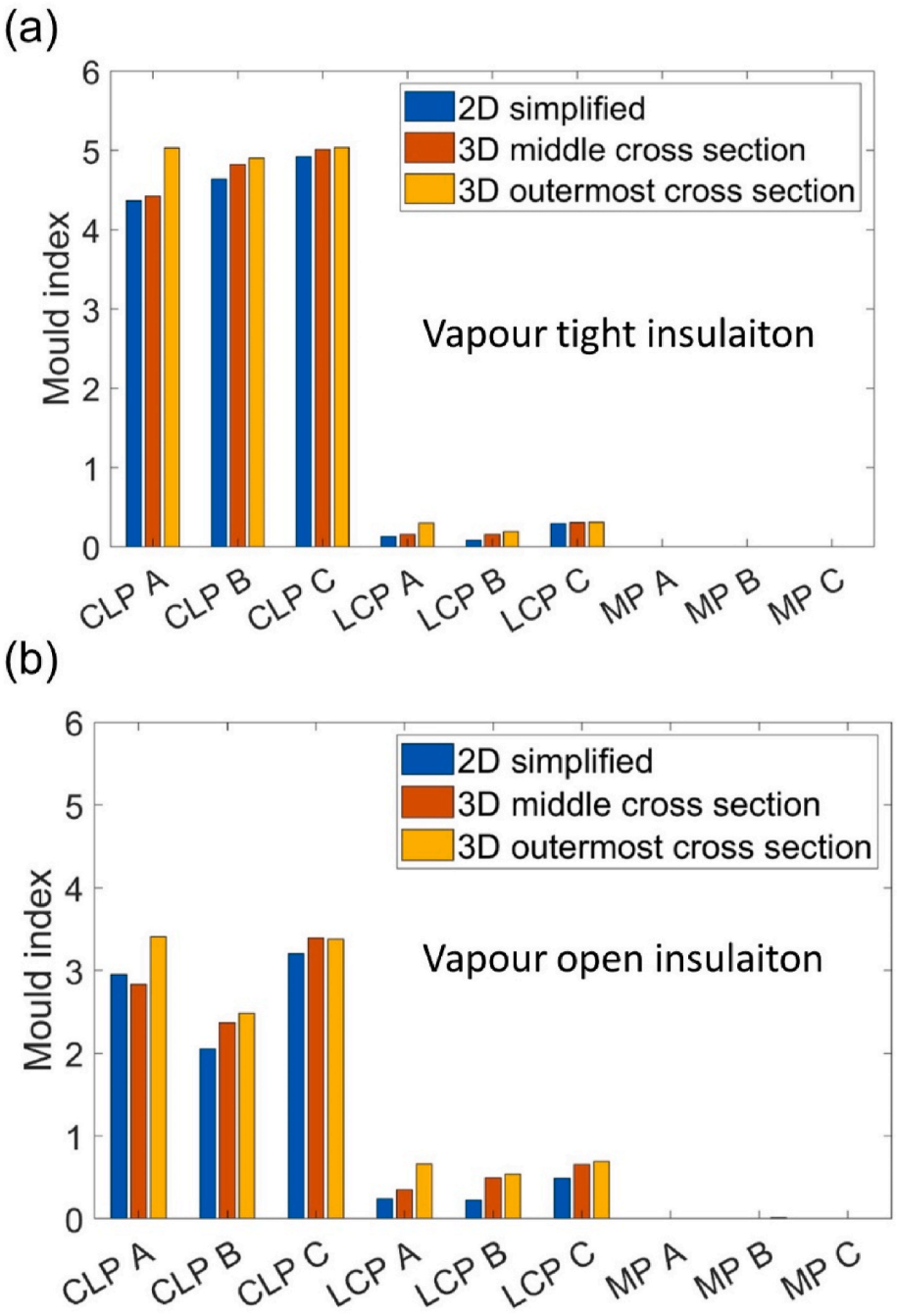

Fig. 12. (a) Maximum mould index at points A, B and C in the 2D model and central and edge cross sections of the 3D model for wall envelopes with vapour-tight insulation (CL cement lime, LC lime cement, M mineral, P plaster); (b) Maximum mould index at points A, B and C in the 2D model and central and edge cross sections of 3D model for wall envelopes with vapour-open insulation.

3.3. Influence of active heating on 2D and 3D models

The effect of actively heating the wooden beam-end is studied here with the 2D and 3D models. Wall envelopes with the render of cement lime plaster demonstrate much higher moisture risk than wall envelopes with the other two renders. For wall envelopes with cement lime plaster, interior insulation with vapour-open insulation will lead to much lower moisture risk than with vapour-tight insulation. Due to the high liquid permeability of the cement lime plaster, a large amount of rainwater can penetrate into the wall envelope. A vapour-open interior system can dry the accumulated moisture in the wall towards both outside and inside environments whereas a vapour-tight insulation system can only dry the accumulated water towards outside environment. Hence the selected wall envelope for analysis here is the vapour-open wall envelope with cement lime plaster as render. Heating plates are applied at the wooden beam end for active heating. A heating flux of 90, 150 and 210 W/m^2 is applied continuously from 1 November to 30 April to increase the wooden beam-end temperature in the cold period. The energy demand for heating plate is:

$$\varphi_H = Q_H \cdot A \cdot t \cdot 2.78 \cdot 10^{-7} \tag{11}$$

where φ_H is the active heating energy demand (kWh), Q_H is the heating flux (W/m^2), A is the size of heating plate, t is the time (s), $2.78 \cdot 10^{-7}$ is the conversion factor from Joules to kWh. With a wooden beam-end area of 0.06 m^2, the total energy demand of the active heating system is 23.5,

39.1 and 54.8 kWh, respectively, for the heating flux of 90, 150 and 210 W/m^2. As a note the energy demand by the active heating represents a very small fraction of the normal heating demand in a building.

Figs. 13 and 14 show the simulated temperature and relative humidity in the 2D model and the central and edge cross sections of the 3D model. The simulated temperature in the 2D model is much higher than those in the 3D model from November to April (Fig. 13). In the other periods when active heating stops, the temperature of the 2D model becomes almost the same as those in the 3D model. Similarly, the relative humidity in the 2D model is much smaller than those in the 3D model over the heating period (Fig. 14). For example, when the active heating flux is 210 W/m^2, the relative humidity at point A in the 2D model varies around 0.2 whereas the RH at the central cross section of the 3D model varies around 0.4 and at the edge cross section of the 3D model around 0.8. The large difference in temperature and relative humidity between the 2D and 3D models is due to the simplification of the wooden beam in the 2D model. In the 2D model, the heat flux is applied over the entire width of the wall envelope, whereas in the 3D model the heating is only active over the area of wooden beam-end. Consequently, the heating effect is much smaller in the 3D model compared with that in the 2D model.

The influence of active heating on temperature is location dependent. At point A in the central cross section of the 3D model, there is a relatively large temperature increase due to the important effect of active heating. However, point A in the 3D edge cross section shows a much smaller temperature increase, due to its proximity to the unheated and colder masonry wall. Points B and C show lower temperatures both at the central or edge cross sections in the 3D model, which are all in proximity to the unheated and colder masonry wall, leading to higher humidity levels.

Fig. 15a compares the temperature distribution on the 18th of January at the central and edge cross sections of the 3D model. The active heating greatly increases the temperature around the wooden beam-end at the 3D central cross section, reaching the highest temperature of 35 °C. However, the region of elevated temperature is quite limited. Due to 3D-dimensional heat flow effects, the center of the wooden beam-end, here shown as the lower part, is much warmer than the upper part. The temperature at the beam-end at the edge cross section is between 13 and 17 °C (Fig. 13), which is much lower compared to the central cross section. The influence of active heating on relative humidity distribution is related to temperature distribution (Fig. 15b). There is a large decrease of relative humidity around the wooden beam-end at the 3D central cross section whereas relative humidity decreases at the edge cross section is much smaller.

Point C at the edge cross section has the highest relative humidity and thus the highest mould risk in the wooden-beam. The magnitude of the active heating flux has very large influence on mould index at this point. The maximum mould index at this point is 2.2, 1.5, 1.1, respectively, for the heating flux of 90, 150 and 210 W/m^2 (Fig. 15c). By comparison, these values are much smaller than the mould index of 3.4 at this point for the same assembly without active heating (Fig. 15c).

It is concluded that the 3D effect is important in assessing the effect of active heating. The hygrothermal performance of wooden beam-end in the internally insulated masonry walls has to be analysed with a 3D model when local heating is considered. Active heating combined with rain protection will greatly reduce the risk of moisture-related problems at a wooden beam-end. The analysis using a 2D model will lead to significant underestimations of moisture damage risk as the heating area in the 2D model is spanning over the total width of the wall, while in the 3D model heating only happens over the width of the wooden beam-end.

4. Discussions

The risk of moisture-related problems at the wooden beam-ends is low when wind-driven rain load on the wall surface is low or a water repellent exterior plaster is used on the wall to protect it against rain. Morelli and Svendsen [2] showed that wind-driven rain has a great influence on moisture content at the wooden beam-end. When the

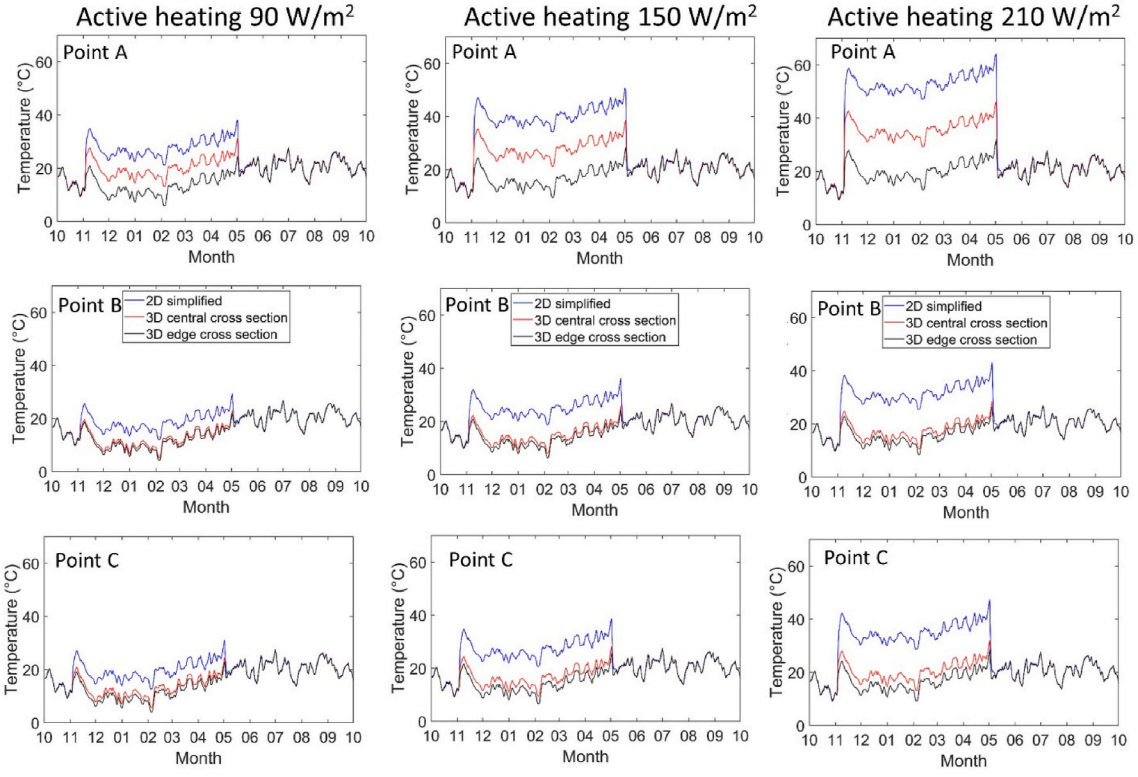

Fig. 13. Temperature at points A, B and C in the 2D model and central and edge cross sections of 3D model for the vapour-open wall envelope with cement lime plaster with active heating at end of wood beam.

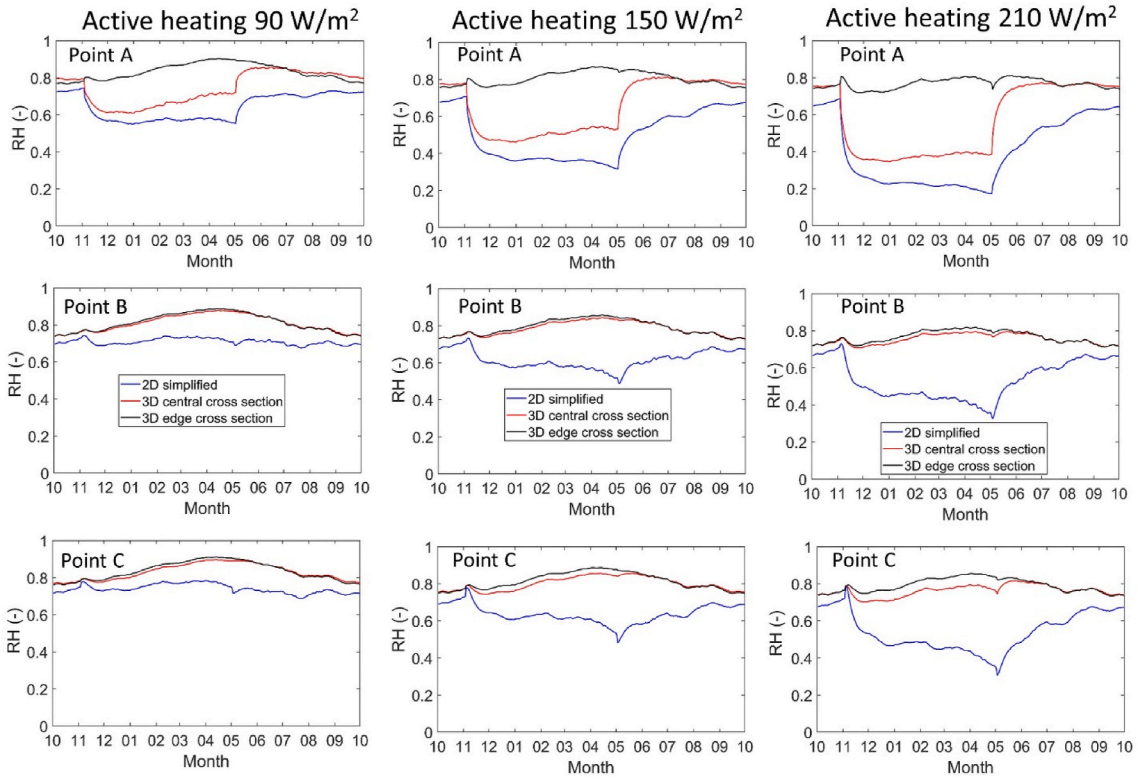

Fig. 14. Relative humidity at points A, B and C in the 2D model and central and edge cross section of 3D model for the vapour-open wall envelope with cement lime plaster.

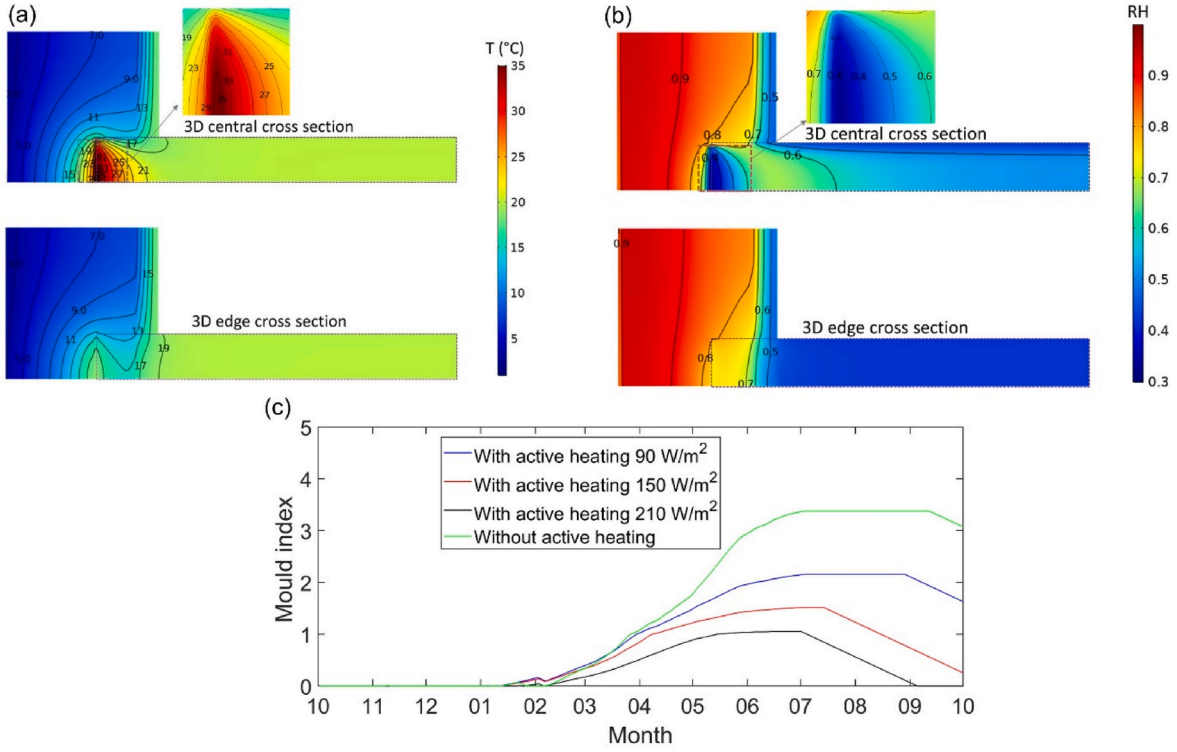

Fig. 15. (a) Temperature distribution at the 3D central and edge cross sections on the 18th of January for the vapour-open wall envelope with cement lime plaster with the active heating flux of 210 W at end of wood beam. The dashed box indicates the location of the wooden beam; (b) Relative humidity at the 3D central and edge cross section on the 18th of January for the vapour-open wall envelope with cement lime plaster with the active heating flux of 210 W at end of wood beam; (c) Mould index at point C at the 3D edge cross section at the end of the wood beam with and without active heating.

wind-driven rain catch ratio is 0.1, there is no moisture risk in the wooden beam-ends. However, when the wind-driven rain catch ratio increases to 0.3, there is moisture risk in the wooden beam-ends. Harrestrup and Svendsen [4] presented that the risk of mould growth at wooden beam-end is larger for façade with higher wind-driven rain load. Kopecky et al. [21] demonstrated that artificial rain load applied on the experimental walls clearly increased the moisture content level in the wooden beam-ends. Dumont et al. [35] measured low moisture content level of 10–15% in wooden elements embedded in an internally insulated house that has a low wind-driven rain load. By comparison, they measured moisture content level above 20% in wood members of an internally insulated house that has moisture penetration due to wet foundation and wind-driven rain. Kehl [11] summarized measurement results in different studies and indicated that moisture content of the wooden beam-ends stays between 10 and 18% for walls with water repellent exterior plaster or with low wind-driven rain load. All these findings are similar to our results that exterior render with larger liquid permeability leads to higher moisture risk in the wooden-beam end. In our study, for the wall envelopes with the exterior renders of lime cement plaster and mineral plaster, moisture content at the wooden beam-ends is also in the range between 10 and 18%.

In the study, it is assumed that there is perfect hydraulic contact at the interface between brick and mortar. However, capillary moisture transport in masonry walls can be strongly affected by the interface resistance between brick and mortar [37–39]. Currently, the experimental studies on interface resistance between brick and mortar are only at the laboratory scale under simplified conditions. There is a need to study the effect of interface resistance in situ in the walls.

5. Conclusions

The hygrothermal performance of a wooden beam-end embedded in an internally insulated masonry wall is compared in this study using 2D and 3D models. The influence of render type and vapour control strategy in 2D and 3D modelling is considered. A 2D model with a detailed distribution of bricks and mortar joints is built. Then a 2D model with a simplified distribution of bricks and mortar joints is built and compared with the detailed 2D model. The simulated results in these two 2D models are found to be very close. Based on the results of the simplified 2D model, a 3D model is developed. The results in the simplified 2D and 3D models are compared. In general, the difference in relative humidity and temperature between the 2D and 3D models is relatively small. The difference in mould index between the 2D and 3D models is also small. Therefore, it is suitable to replace 3D models with 2D ones for predicting the risk of mould problems in the wood beam-end. However, for evaluating the effect of active local heating on the moisture risk at wooden beam-end, a 3D hygrothermal model has to be used, since the effect of heating will be seriously overpredicted in a 2D hygrothermal model.

Declaration of competing interest

The authors declare that they have no known competing financial interests or personal relationships that could have appeared to influence the work reported in this paper.

Acknowledgement

This research project is part of the Swiss Competence Center for Energy Research SCCER FEEB&D of the Swiss Innovation Agency Innosuisse (CTI.1155002539). We would like to thank MeteoSwiss for providing the meteorological data.

References

[1] E.J. de Place Hansen, K.B. Wittchen, Energy savings due to internal façade insulation in historic buildings, in: 3rd Int. Conf. Energy Effic. Hist. Build. (EEHB2018), Visby, Sweden, Sept. 26th to 27th, 2018, pp. 22–31. Uppsala University, 2018.
[2] M. Morelli, S. Svendsen, Investigation of interior post-insulated masonry walls with wooden beam ends, J. Build. Phys. 36 (2013) 265–273, https://doi.org/10.1177/1744259112447928.
[3] M. Guizzardi, J. Carmeliet, D. Derome, Risk analysis of biodeterioration of wooden beams embedded in internally insulated masonry walls, Construct. Build. Mater. 99 (2015) 159–168, https://doi.org/10.1016/j.conbuildmat.2015.08.022.
[4] M. Harrestrup, S. Svendsen, Internal insulation applied in heritage multi-storey buildings with wooden beams embedded in solid masonry brick façades, Build. Environ. 99 (2016) 59–72, https://doi.org/10.1016/j.buildenv.2016.01.019.
[5] X. Zhou, D. Derome, J. Carmeliet, Hygrothermal modeling and evaluation of freeze-thaw damage risk of masonry walls retrofitted with internal insulation, Build. Environ. 125 (2017) 285–298, https://doi.org/10.1016/j.buildenv.2017.08.001.
[6] X. Zhou, J. Carmeliet, D. Derome, Influence of envelope properties on interior insulation solutions for masonry walls, Build. Environ. 135 (2018) 246–256, https://doi.org/10.1016/j.buildenv.2018.02.047.
[7] X. Zhou, J. Carmeliet, D. Derome, Assessment of risk of freeze-thaw damage in internally insulated masonry in a changing climate, Build. Environ. 175 (2020) 106773.
[8] E. Vereecken, S. Roels, Capillary active interior insulation: do the advantages really offset potential disadvantages? Mater. Struct. 48 (2015) 3009–3021.
[9] N.F. Jensen, T.R. Odgaard, S.P. Bjarløv, B. Andersen, C. Rode, E.B. Møller, Hygrothermal assessment of diffusion open insulation systems for interior retrofitting of solid masonry walls, Build. Environ. (2020) 107011.
[10] L. Wang, H. Ge, Stochastic modelling of hygrothermal performance of highly insulated wood framed walls, Build. Environ. 146 (2018) 12–28.
[11] D. Kehl, U. Ruisinger, R. Plagge, J. Grunewald, Wooden Beam Ends in Masonry with Interior Insulation–A Literature Review and Simulation on Causes and Assessment of Decay, CESBP Vienna, 2013, pp. 299–304.
[12] M. Morelli, M.A. Lacasse, A systematic methodology for design of retrofit actions with longevity, J. Build. Phys. 42 (2019) 585–604.
[13] M. Vanpachtenbeke, J. Langmans, J. Van den Bulcke, J. Van Acker, S. Roels, Modelling moisture conditions behind brick veneer cladding: verification of common approaches by field measurements, J. Build. Phys. (2020), 1744259120908283.
[14] C. Hall, W.D. Hoff, Water Transport in Brick, Stone and Concrete, CRC Press, 2009, https://doi.org/10.1520/cca10518j.
[15] L. Havinga, H. Schellen, The impact of convective vapour transport on the hygrothermal risk of the internal insulation of post-war lightweight prefab housing, Energy Build. 204 (2019) 109418.
[16] C. Carll, A.C. Wiedenhoeft, Moisture-related properties of wood and the effects of moisture on wood and wood products, Moisture Control Build, in: Key Factor Mold Prev, second ed., PA ASTM Int., West Conshohocken, 2009, pp. 54–79.
[17] H.M. Künzel, H. Künzel, A. Holm, Rain protection of stucco facades. Proc. Therm. Perform. Exter. Envel. Whole Build. IX–International Conf., 2004, p. 7.
[18] M. Pazera, M. Bomberg, Applying lessons from clay-brick veneer to design a stucco mix, in: BEST Conf. Build. Enclos. Sci. Technol., 2010.
[19] H.M. Künzel, Effect of interior and exterior insulation on the hygrothermal behaviour of exposed walls, Mater. Struct. 31 (1998) 99–103.
[20] P. Wegerer, T. Bednar, Improving Durability of Wooden Beam Bearings in inside Insulated Walls by Tempering the Beam's Heads, in: Proc. IBPC2018, 2018. Syracuse, NY.
[21] P. Kopecký, K. Staněk, M. Bureš, J. Richter, P. Ryparová, J. Tywoniak, Experimental investigations of wooden beam ends in masonry with interior insulation: measured data in real-scale experimental walls exposed to semi-continental climatic conditions, J. Build. Phys. 43 (2019) 147–170.
[22] E. Vereecken, S. Roels, Wooden beam ends in combination with interior insulation: an experimental study on the impact of convective moisture transport,, Build. Environ. 148 (2019) 524–534.
[23] P. Johansson, S. Geving, C.E. Hagentoft, B.P. Jelle, E. Rognvik, A.S. Kalagasidis, B. Time, Interior insulation retrofit of a historical brick wall using vacuum insulation panels: hygrothermal numerical simulations and laboratory investigations, Build. Environ. 79 (2014) 31–45, https://doi.org/10.1016/j.buildenv.2014.04.014.
[24] C.-E. Hagentoft, A.S. Kalagasidis, B. Adl-Zarrabi, S. Roels, J. Carmeliet, H. Hens, J. Grunewald, M. Funk, R. Becker, D. Shamir, Assessment method of numerical prediction models for combined heat, air and moisture transfer in building components: benchmarks for one-dimensional cases, J. Therm. Envelope Build. Sci. 27 (2004) 327–352.
[25] M. Guizzardi, Hygrothermal Performance Assessment of Novel Interior Insulation Solutions, PhD thesis, ETH Zurich, 2014.
[26] H.M. Künzel, in: Simultaneous Heat and Moisture Transport in Building Components, One-And Two-Dimensional Calc. Using Simple Parameters. IRB-Verlag Stuttgart, 1995.
[27] W. Durner, Predicting the unsaturated hydraulic conductivity using multi-porosity water retention curves, Indirect Methods Estim. Hydraul. Prop. Unsaturated Soils. (1992) 185–202.
[28] M.T. van Genuchten, A closed-form equation for predicting the hydraulic conductivity of unsaturated Soils1, Soil Sci. Soc. Am. J. 44 (1980) 892, https://doi.org/10.2136/sssaj1980.03615995004400050002x.
[29] H. Janssen, B. Blocken, J. Carmeliet, Conservative modelling of the moisture and heat transfer in building components under atmospheric excitation, Int. J. Heat Mass Tran. 50 (2007) 1128–1140, https://doi.org/10.1016/j.ijheatmasstransfer.2006.06.048.

[30] X. Zhou, D. Derome, J. Carmeliet, Robust moisture reference year methodology for hygrothermal simulations, Build. Environ. 110 (2016) 23–35, https://doi.org/10.1016/j.buildenv.2016.09.021.
[31] E.N, Hygrothermal Performance of Building Components and Building Elements–Assessment of Moisture Transfer by Numerical Simulation, 2007, 15026.
[32] A. TenWolde, ASHRAE Standard 160P-Ccriteria for Moisture Control Design Analysis in Buildings, 2008.
[33] H.M. Künzel, K. Kiessl, Calculation of heat and moisture transfer in exposed building components, Int. J. Heat Mass Tran. 40 (1996) 159–167.
[34] A. Hukka, H.A. Viitanen, A mathematical model of mould growth on wooden material, Wood Sci. Technol. 33 (1999) 475–485.
[35] R. Dumont, L. Snodgrass, J. Kokko, J. Goth, C. Schumacher, Field measurement of wood moisture contents in wood joists embedded in masonry exterior walls, in: Proc. 10th Annu. Conf. Build. Sci. Technol., 2005.
[36] K. Ueno, J.W. Lstiburek, P. Eng, Field monitoring of embedded wood members in insulated masonry walls in a cold climate. Proc. BEST4 Conf., 2015.
[37] H. Derluyn, H. Janssen, J. Carmeliet, Influence of the nature of interfaces on the capillary transport in layered materials, Construct. Build. Mater. 25 (2011) 3685–3693, https://doi.org/10.1016/j.conbuildmat.2011.03.063.
[38] X. Zhou, G. Desmarais, P. Vontobel, J. Carmeliet, D. Derome, Masonry brick–cement mortar interface resistance to water transport determined with neutron radiography and numerical modeling, J. Build. Phys. (2020), 1744259120908967.
[39] K. Calle, T. De Kock, V. Cnudde, N. Van den Bossche, Liquid moisture transport in combined ceramic brick and natural hydraulic lime mortar samples: does the hygric interface resistance dominate the moisture transport? J. Build. Phys. 43 (2019) 208–228.